New Copper (II) Isomer Based on 8-aminoquinoline Ligand: Synthesis, Molecular Structure, Hirshfeld Surface Analysis and Computational Study.

Zouaoui Setifi
Universite Ferhat Abbas Setif 1
Hela Ferjani (Ferjani97@ymail.com)
Imam Mohammad Ibn Saud University https://orcid.org/0000-0001-8048-847X
Youssef Ben Smida
University of 7th November at Carthage: Universite de Carthage
Christian Jelsch
University of Lorraine: Universite de Lorraine
Fatima Setifi
Universite Ferhat Abbas Setif 1
Christopher Glidewell
St Andrews University
Ferjani Hela
Imam Muhammad Ibn Saud Islamic University

Research Article

Keywords: Crystal structure, New Copper (II) isomer, non-Covalent interactions, Hirshfeld surface analysis, Reactivity descriptors, Fukui functions

Posted Date: November 9th, 2021

DOI: https://doi.org/10.21203/rs.3.rs-1026699/v1

New Copper (II) isomer based on 8-aminoquinoline ligand: Synthesis, molecular structure, Hirshfeld surface analysis and computational study.

Zouaoui Setifi[1,2], Hela Ferjani[3,*], Youssef Ben Smida[4], Christian Jelsch[5], Fatima Setifi[1,*], Christopher Glidewell[6],

[1]Laboratoire de Chimie, Ingénierie Moléculaire et Nanostructures (LCIMN), Université Ferhat Abbas Sétif 1, Sétif 19000, Algeria

[2]Département de Technologie, Faculté de Technologie, Université 20 Août 1955-Skikda, Skikda 21000, Algeria

[3]Chemistry Department, College of Science, IMSIU (Imam Mohammad Ibn Saud Islamic University), Riyadh 11623, Kingdom of Saudi Arabia

[4]Laboratory of Valorization of Useful Materials, National Center of Materials Sciences Research, Techno Park Borj Cedria, Carthage University, Soliman, Tunisia.

[5]CRM2 , CNRS, Institut Jean Barriol, Université de Lorraine, 54000, Nancy, France

[6]School of Chemistry, University of St Andrews, St Andrews, Fife, KY16 9ST, UK

Corresponding authors: hhferjani@imamu.edu.sa (Hela Ferjani); fat_setifi@yahoo.fr (Fatima Setifi)

ABSTRACT

Toward the treating of a multifunctional material, new $[Cu(H_2O)_2(C_9H_8N_2)_2]Cl_2$ isomer **1** has been synthesized by solvothermal method. The single-crystal X-ray study, Hirshfeld surface analysis and computational calculation were discussed. Hydrogen bonding network within the complex enable the formation of 3D network supported by aromatic stacking interactions of quinoline rings in face-to-face and edge-to face fashions. The analysis of Hirshfeld surfaces, facilitate a comprehension of intermolecular interactions in the structure. The enrichment ratio (E) was calculated to examine the propensity of intermolecular interactions to form contacts in crystals. It shows that the favorable contacts responsible for the crystal packing are strong hydrogen bonds and stacking interactions. The reactivity descriptors for **1** such as E_{HOMO} and E_{LUMO} energies, ionization potential (IP), Electron affinity (EA), Mulliken electronegativity (χ) and the Absolute hardness (η) was calculated by PBE functional method with DNP basis set. The possible sites for nucleophilic and electrophilic attacks on **1** were analyzed through Fukui functions.

Keywords: Crystal structure; New Copper (II) isomer; non-Covalent interactions; Hirshfeld surface analysis; Reactivity descriptors; Fukui functions.

Introduction

As a result of their ability to bind metal ions in various ways, pseudohalide and polynitrile anions, either working alone or in combination with neutral co-ligands, provide opportunities for the generation of molecular architectures with different dimensions and topologies [1-8]. 8-Aminoquinoline is a pyridine derivative in which aniline is fused with pyridine so that a N,N' chelating motive may be generated. 8-Aminoquinoline and its derivatives are systems that have been recently undertaken, because of their antiprotozoal activities and other

medicinal properties [9-11]. They have also been used to prepare new adjustable molecular materials [12-14]. Different functionalized molecules of 8- aminoquinoline have been described [15-17]. However, the coordination chemistry of 8-aminoquinoline, as such, is less cited in the literature [18, 19]. Dicyanamide pseudohalide (N(CN)2-, dca) has been used frequently to synthesize a wide range of coordination polymers with fascinating structural and magnetic properties. The richness of its coordination chemistry is due to the various binding modes it presents. In view of this coordination capacity, this ligand has also been explored for its usefulness in the development of materials capable of coupling by magnetic exchange. It was during attempts to prepare such complexes with 8-aminoquinoline as a co-ligand that the title complex was unexpectedly obtained. Therefore, here we report the synthesis and detailed studies of a novel copper (II) complex bearing an aqin ligand (aqin=8-aminoquinoline) by single crystal X-ray crystallography and computational methods.

Experimental

Materials and Synthesis

All chemicals were furnished from commercial sources and used without further purification. The compound **1** was prepared by solvothermal synthesis under autogenous pressure.

A mixture of copper (II) chloride dihydrate (17 mg, 0.1 mmol), 8-aminoquinoline (29 mg; 0.2 mmol) and sodium dicyanamide (18 mg, 0.2 mmol) in H_2O/MeOH (3:1 v/v, 20 ml) was agitated for 30 min and moved to Teflon-lined autoclave. The autoclave is then heated at 180 °C for 3 days. After slowly cooling at a rate of 10 °C/h at room temperature, light violet crystals of 1 were obtained, and are suitable for the of X-ray diffraction study.

X-ray crystallography

The X-ray diffraction data were collected at 100 K using an Agilent Xcalibur Sapphire1 diffractometer, equipped with a graphite-monochromatized Mo *K*α radiation (λ= 0.71073 Å). A multi-scan [20] absorption correction was applied. The structure was solved and refined by full-matrix least squares based on F^2 using SHELXS-97 and SHELXL-97 [21], respectively. The hydrogen atoms were treated as riding atoms and refined with N-H, O-H and C-H distances fixed at 0.89, 0.83 and 0.95 Å, respectively, with U_{iso} (H) values of $1.2U_{eq}$ (N, O and C). The molecular graphics were prepared using *Diamond 3* program [22].

Table 1 Crystal data and structure refinement parameters for 1.

Empirical formula	**$[Cu(H_2O)_2(C_9H_8N_2)_2].2Cl$**
Formula weight (g/mol)	458.82
Crystal system, space group	Monoclinic, $P2_1/n$
***a* (Å)**	8.3834 (7)
***b* (Å)**	7.8236 (6)
***β* (°)**	102.594 (8)°
***V* (Å^3)**	942.60 (13)
***μ* (mm^{-1})**	1.46
D_x (Mg m^{-3})	1.617
***F*(000)**	470
Crystal size (mm)	0.35 × 0.30 × 0.05
Crystal habit	Plate, light purple

θ_{min} / θ_{max} (deg)	3.9/27.6°
Measured reflections	5574
Independent reflections	2164
Observed refl. with I> 2σ(I)	1843
R_{int}	0.039
Data/restraints/parameters	2164 /4/136
$R[F^2 > 2\sigma(F^2)]$	0.038
$wR(F^2)$	0.086
GooF=*S*	1.06
$\Delta\rho_{max}$ / $\Delta\rho_{min}$ (e.Å^{-3})	0.44 /-0.42
CCDC Number	2054557

Theoretical methods

Hirshfeld surface calculations

The contacts proportions on the Hirshfeld surface and their enrichment were computed with the MoProViewer software [23]. The contact enrichment ratio E_{xy} between chemical species X and Y is obtained by comparing the actual contacts C_{xy} in the crystal with those computed as if all types of contacts were equiprobable. The nature of contacts and their enrichment in the crystal packing are shown in Table 5. To obtain an integral Hirshfeld surface around each moiety (Cu(II) cation, chloride anion and organic ligand), a set of entities not in contact with each other were selected in the crystal packing.

Computational details

The Frontier Molecular Orbitals HOMO (Highest Occupied Molecular Orbital energy) and LUMO (Lowest Unoccupied Molecular Orbital energy) and the Fukui indices of the asymmetric unit of 1have been obtained by using DMol^3 code [24]. The calculations were carried out by means of Mulliken population analysis [25] and by using the PBE functional method with DNP basis set [26]. The convergence parameters were as follows: maximum displacement 0.005 Å, SCF tolerance 1×10^{-6} eV/atom and convergence energy tolerance 1×10^{-6} Ha.

Results and Discussion

X-ray diffraction study

X-ray crystal structure analysis reveals that **1** crystallizes in the monoclinic space group $P2_1/n$. The asymmetric unit comprises one half of the complex cation $[Cu(H_2O)_2(C_9H_8N_2)_2]^{2+}$ and one chloride counter-anion (Figure 1). The Cu^{II} atom lies on an inversion center (Figure 2). In the cation complex, the Cu^{II} atom is coordinated in a slightly distorted octahedral manner by four N atoms from two chelating 8-aminoquinoline ligands and two axially coordinated water molecules. The N1-Cu-N1^i and N2-Cu-N2^i angles [symmetry code: (i) -x+1, -y+1, -z+1] are linear (180°). The *cis* bond angles around the Cu^{II} atom range from 83.44 (8)-96.56 (8) Å. The Cu-N bond lengths range from 2.007 (2) to 2.023 (2) Å (Table 2). These bond lengths are like those observed in similar structures containing 8-aminoquinoline ligands [27-29]. The axial Cu-OW1 bond (2.431(17) Å) is remarkably longer than the equatorial Cu-N distances (Table 2) because of the Jahn-Teller effect [30]. The 8-aminoquinoline ligands exhibit a *planar* coordination mode in which the angle between the planes defined by the Cu/N1/C9/C8/N2 and N2/C8/C9/N1 of the 8-aminoquinoline ligand is 7.37 (7)º (Figure 3).

Non-covalent interactions such as hydrogen-bonding interactions and aromatic stacking interactions provide extreme stability to the structure. Chloride anions are linked to the cationic complex through two sets of strong hydrogen bonds: two N2-H21/22···Cl1$^{ii/iii}$ {(ii)= -*x*+$^{3}/_{2}$, *y*-½, -*z*+$^{3}/_{2}$; (iii) = *x*-½, -*y*+½, *z*-½} with the amino protons of the NH2-quinoline ligand and two O1W-H11/12···Cl1/Cl1^{ii} with the coordinated water molecules, forming two-dimensional hydrogen-bonding network (Figure 4a, Table 3). The cationic complexes situated around *z*=½ are connected through face-to-face stacking interaction between the quinoline rings {Cg3-Cg3^{i} = 3.521 (3), Cg3-Cg4^{i} = 3.839 (4) Å where Cg3 is the centroid of the ring N1-C9, Cg4 is the centroid of the ring C4-C9; i: symmetry code: -x,1-y,1-z } (Figure 4b) and by edge-to-face stacking interaction between the quinoline rings placed in z=0 and z=½ {Cg4-Cg3^{i} = 4.431 (3), i: symmetry code: -x,1-y,1-z } (Figure 4c). The facility to undergo hydrogen bonds and stacking interactions are a suitable tool in the formation of a self-assembled structure.

The structure of 1represents another isomer of a previously reported structure of [Cu($C_9H_8N_2$)$_2$(Cl)(H_2O)]$^{+}$.(Cl^{-}).H_2O [31] **2** (Figure 5). The single crystal X-ray diffraction analysis of isomers **1** and **2** reveals that their space groups, unit cell parameters, and *Z* values follow a different symmetry order. When comparing the structural parameters of isomers **1** and **2**, the similarity in the two complexes is reflected in the coordinative copper (II) center with two bidentate chelating 8-aminoquinoline. And the difference between the two structures is related to their occupancy of vertices axes. However, the chloride anion and water molecules, in the isomer (2) assumes the roles of the counter anion and coordinative ligands, respectively. The Cu-N (1.985 (9)-2.042(9) Å) and Cu-O (2.566(6) Å) bond lengths are in the normal ranges, though with some differences. The crystal packing of isomers **1** and **2** is stabilized through different hydrogen bonding interactions of type N-H···Cl and O-H···Cl. In the isomer **2**, there is a supplementary N-H···O hydrogen bond between the non-coordinated water molecule and the chloride anions.

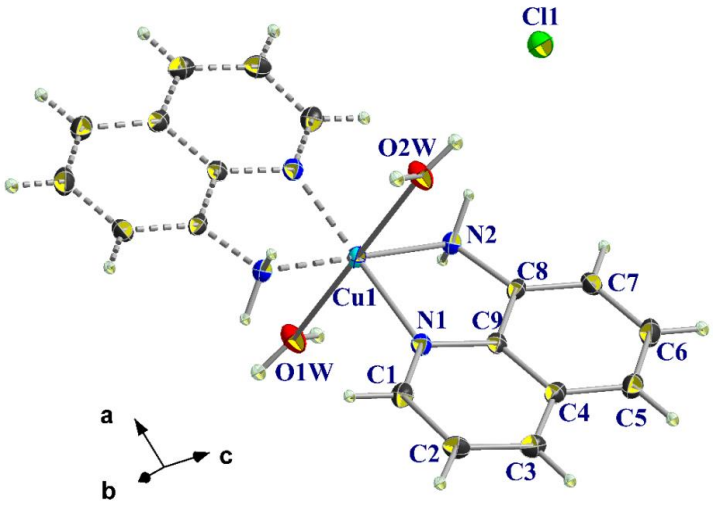

Figure 1. A view of the molecular structure of **1**, with atom labelling. Displacement ellipsoids are drawn at the 50% probability level. Unlabeled atoms (dashed bonds) are related to the labelled atoms by inversion symmetry (Symmetry operation: 1-x, 1-y, 1-z).

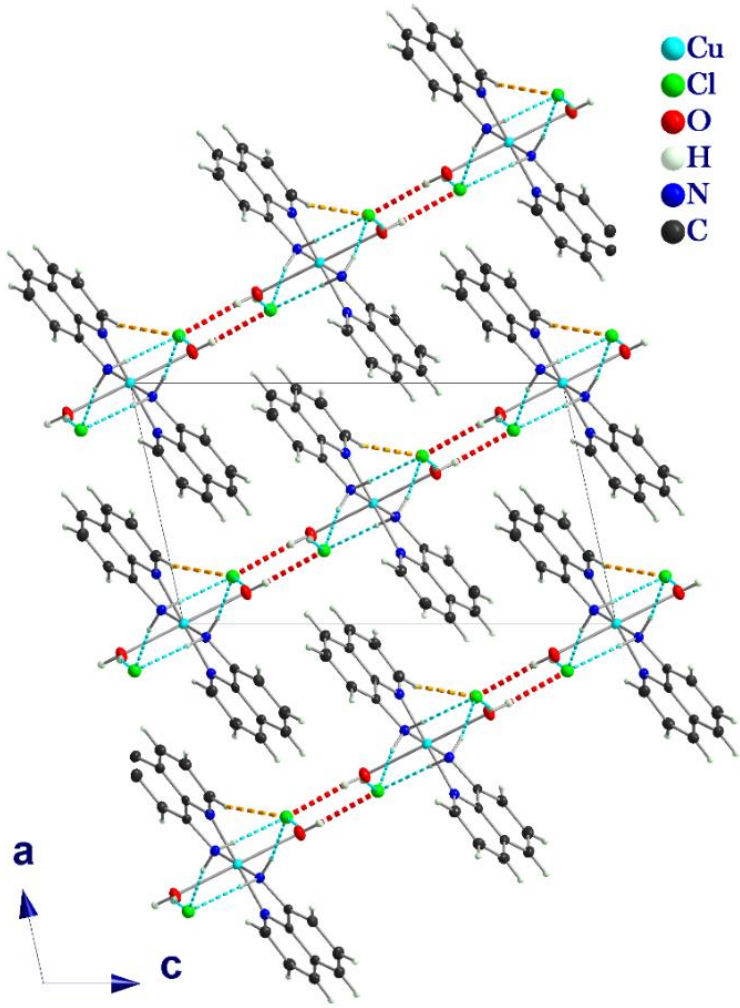

Figure 2. A view of the crystal packing of **1**, showing the alternating cationic complex chains and chlorine anions connected through hydrogen bonds.

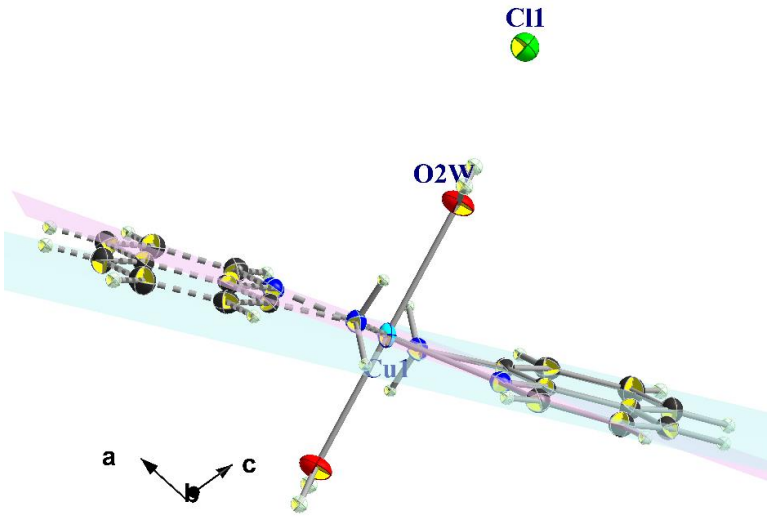

Figure 3. A planar coordination mode of 8-aminoquinoline ligand (Angles between pink and blue planes =7.37 (7)°).

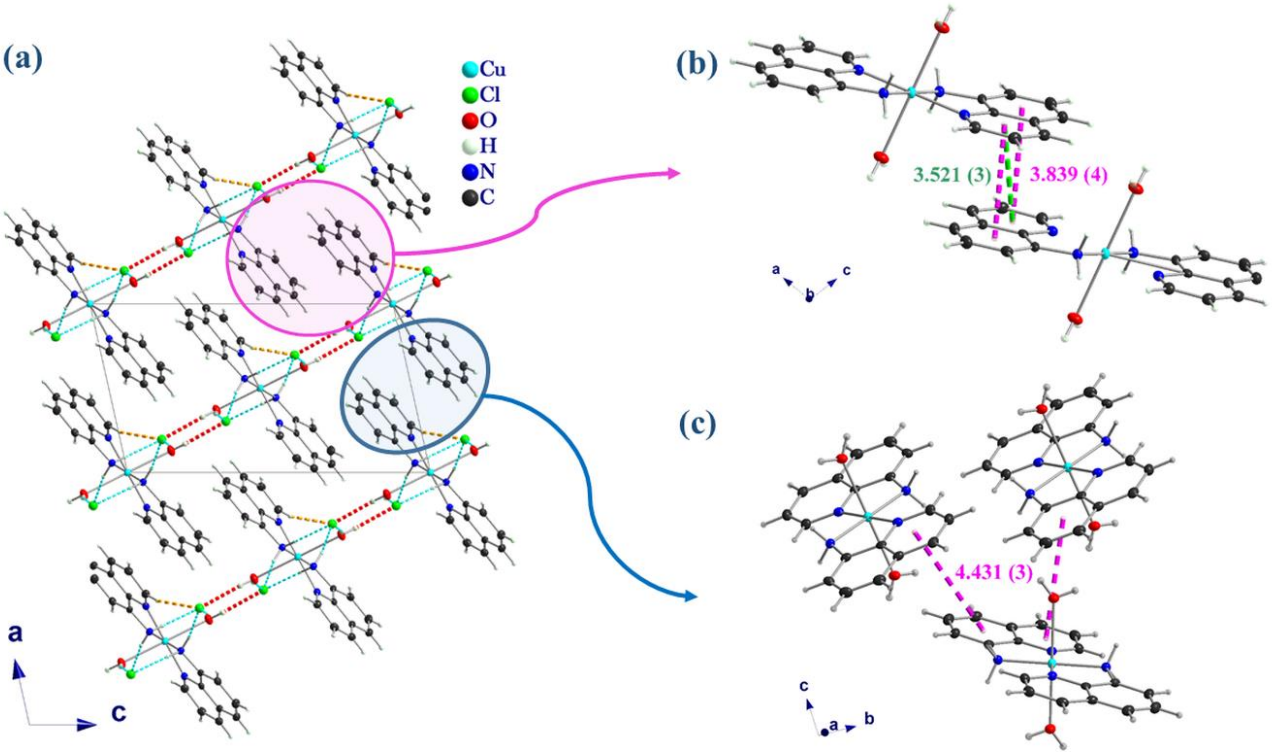

Figure 4. (a) View along *b* axis of the packing diagram showing hydrogen- bonding interactions (cyan and red dashed lines) **(b)** Face-to-Face stacking interactions and **(c)** Edge-to-Face stacking interaction (green and pink dashed lines).

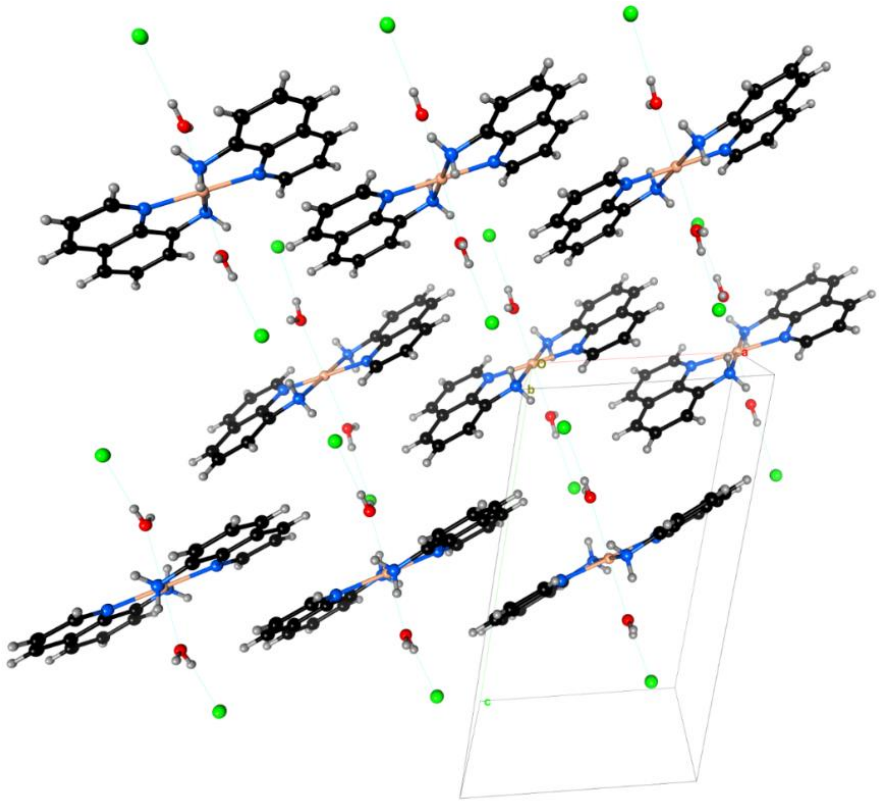

Figure 5. Crystallographic autostereogram of the crystal packing along the *b* axis. HOH···Cl^- hydrogen bonds and O···Cu coordination bonds are shown as dotted lines.

Table 2 Selected bond lengths (Å) and angles (º) for **1**.

Bond lengths (Å)			
Cu1-N2^i	2.007 (2)	C1-C2	1.408 (3)
Cu1-N2	2.007 (2)	C2-C3	1.369 (4)
Cu1-N1^i	2.023 (2)	C3-C4	1.407 (4)
Cu1-N1	2.023 (2)	C4-C5	1.416 (3)
Cu1-O1W^i	2.431 (2)	C4-C9	1.420 (3)
Cu1-O1W	2.431 (2)	C5-C6	1.359 (4)
N1-C1	1.315 (3)	C6-C7	1.407 (4)
N1-C9	1.365 (3)	C7-C8	1.361 (3)
N2-C8	1.448 (3)	C8-C9	1.414 (3)
Angles (º)			
N2^i-Cu1-N2	**180.0**	**N1-C1-C2**	**123.2 (2)**
N2^i-Cu1-N1^i	83.44 (8)	C3-C2-C1	119.3 (2)
N2-Cu1-N1^i	96.56 (8)	C2-C3-C4	119.3 (2)
N2^i-Cu1-N1	96.56 (8)	C3-C4-C5	124.3 (2)
N2-Cu1-N1	83.44 (8)	C3-C4-C9	117.6 (2)
N1^i-Cu1-N1	180.0	C5-C4-C9	118.1 (2)
N2^i-Cu1-O1W^i	88.50 (7)	C6-C5-C4	120.8 (2)
N2-Cu1-O1W^i	91.50 (7)	C5-C6-C7	120.7 (2)
N1^i-Cu1-O1W^i	84.19 (7)	C8-C7-C6	120.4 (2)
N1-Cu1-O1Wi	95.81 (7)	C7-C8-C9	120.1 (2)
N2^i-Cu1-O1W	91.50 (7)	C7-C8-N2	124.3 (2)

N2-Cu1-O1W	88.50 (7)	C9-C8-N2	115.7 (2)
N1^{i}-Cu1-O1W	95.81 (7)	N1-C9-C8	117.9 (2)
N1-Cu1-O1W	84.19 (7)	N1-C9-C4	122.2 (2)
O1Wi-Cu1-O1W	180.0	C8-C9-C4	119.9 (2)
C1-N1-C9	118.4 (2)		
C1-N1-Cu1	129.74 (18)		
C9-N1-Cu1	111.55 (16)		
C8-N2-Cu1	109.89 (15)		

Symmetry code: *(i)* -*x*+1, -*y*+1, -*z*+1.

Table 3 Hydrogen bond and short inter-ion contact geometry in **(1)**.

D*–H···*A	***D*-H**	***H*···*A***	***D*···*A***	***D*-H···*A***
O1W-H11···Cl1	0.83	2.32	3.136 (2)	166
O1W-H12···Cl1^{ii}	0.83	2.33	3.151 (2)	165
N2-H22···Cl1^{ii}	0.88	2.49	3.294 (2)	154
N2-H21···Cl1^{iii}	0.89	2.36	3.245 (2)	174

Symmetry codes : (ii) -*x*+$^{3}/_{2}$, *y*-½, -*z*+$^{3}/_{2}$; (iii) *x*-½, -*y*+½, *z*-½ ; (iv) x-½, $^{3}/_{2}$-y, z -½

Interactions and Hirshfeld surface analysis

The most abundant contacts are constituted by the O/N···HCl^{-} strong hydrogen bonds followed by the weaker C···H-C and C-H···Cl^{-} weak hydrogen bonds (Table 3). All the favorable interactions are over-represented, notably the strong H-bonds (*E*=3.5). The chloride anion is completed surrounded by hydrogen atoms from the organic and the water molecules. The copper cation has no contact with the chloride anion but is instead coordinated by the water oxygen and two nitrogen atoms and these contacts are the most enriched at high ratios *E*>5.7. In a crystal structure [31] of 8-aminoquinoline $CuCl_2$, devoid of water, the copper (II) cation is conversely coordinated by two nitrogen atoms and two chloride anions [32].

The C···C contacts are the third abundant type (Figure 6) and are remarkably enriched (*E*=2.57) due to extensive aromatic stacking between the 8-aminoquinoline molecules. The planar aromatic moieties show two orientations (forming an angle of 37.0°) in the crystal packing (Figure 5). The self-contacts are absent or strongly under-represented, except for the C···C type.

The Hirshfeld surface appear to have an equal share of hydrophobic (Hc and C) and hydrophilic (more charged) atoms. The crystal is constituted by an alternance of hydrophobic and hydrophilic layers parallel to the (*b*, *a*+*c*) plane (Figure 6). This can be seen in the contact statistics as both hydrophobic and hydrophilic contacts are enriched at *E*≅1.35. On the other hand, the cross contacts are disfavored at *E*=0.65 and consist mostly of weak C-H···Cl^{-} hydrogen bonds.

The fingerprint plots (Figure 7) show two spikes at short distance constituted by the N···Cu coordination and the N-H···Cl strong hydrogen bonds.

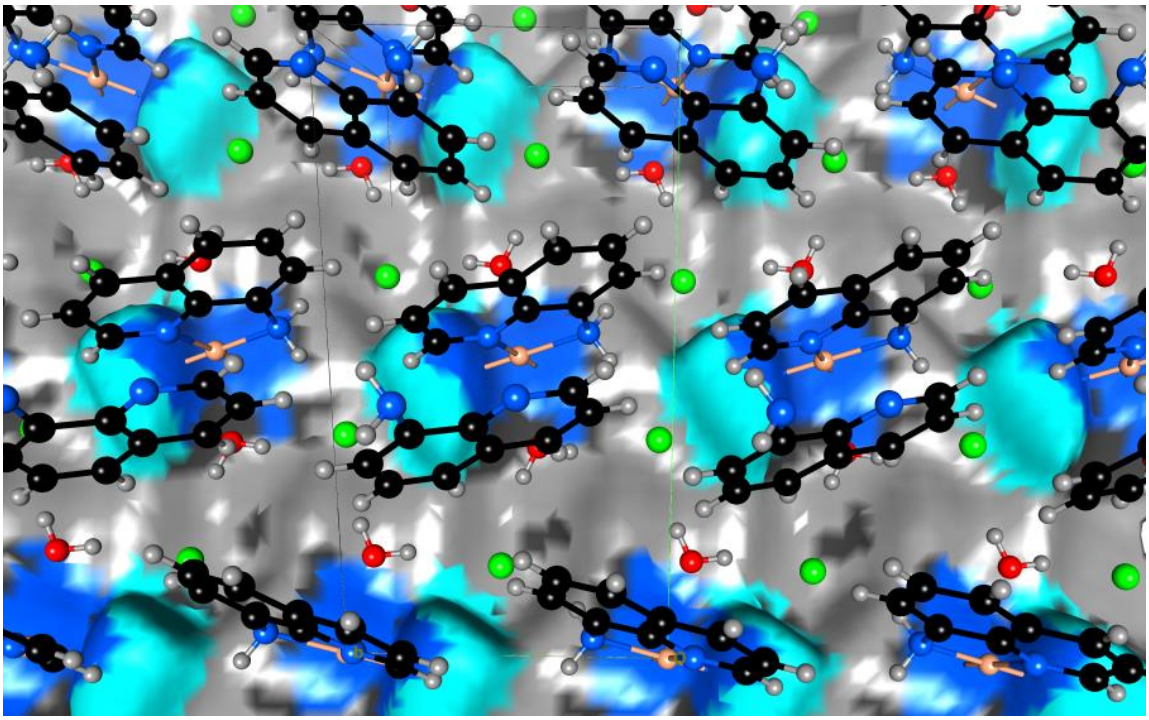

Figure 6. Autostereogram of the Hirshfeld surface over an organic layer parallel to the (***b***, ***a***+***c***) plane. The unit cell is shown, and the ***b*** axis is horizontal, the ***c*** axis vertical. Surface color: grey: Hc, blue: nitrogen; light blue: Hn, dark grey: carbon. Oxygen and chlorine atoms are in red and green, respectively.

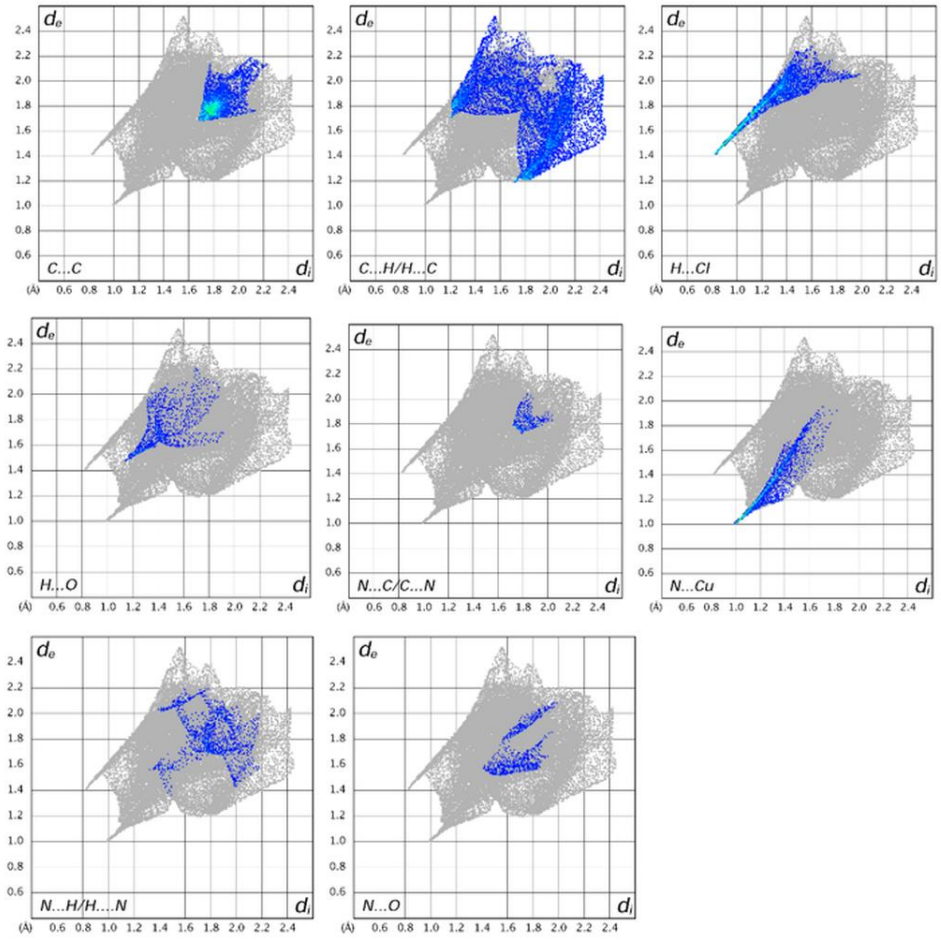

Figure 7. Fingerprint plot of the main interactions around the 8-aminoquinoline ligand.

Table 4 Analysis of contacts on the Hirshfeld surface. Reciprocal contacts X⋯Y and Y⋯X are merged. The second line shows the chemical content on the surface. The % of contact types between chemical species is given followed by their enrichment ratio. The major contacts as well as the major enriched ones are highlighted in bold characters. The hydrophobic hydrogen atoms bound to carbon (Hc) were distinguished from the more polar ones bound to oxygen or nitrogen (Ho/n). In the last 3 lines, the contacts have been regrouped in terms of hydrophobic atoms (C and Hc) and hydrophilic (the others).

Atom	**Ho/n**	**C**	**N**	**O**	**Cl**	**Cu**	**Hc**
Surface %	**16.6**	**24.1**	**5.7**	**4.8**	**16.1**	**6.3**	**26.3**
Ho/n	1.1						
C	0.8	**13.8**			% contacts		
N	0.0	0.5	0.0				
O	0.1	0.5	0.3	0.0			
Cl	**19.9**	1.5	0.0	0.0	0.0		
Cu	1.3	0.9	**7.2**	3.7	0.0	0.0	
Hc	**8.8**	**16.7**	0.4	2.6	**15.9**	0.4	3.5

Ho/n	0.41						
C	0.11	**2.57**			Rxy		
N	0	0.15	0				
O	0.04	0.21	0.39	0			
Cl	**3.5**	0.19	0	0	0		
Cu	0.64	0.3	**7.8**	**5.7**	0	0	
Hc	1.11	**1.47**	0.11	1.04	**1.83**	0.13	0.59
% surface	hydro-	50.5	Hydro-	49.5			
% contacts	phobic	34.0	philic	33.6	Cross	32.4	
Enrichment		1.34		1.37		0.65	

Molecular descriptors and Fukui indices

Calculated descriptors

The Frontier Molecular Orbitals (HOMO and LUMO) and their energies are very useful for chemists, and they are very important in quantum chemistry. They are used to determine the most reactive position in electronic systems and explain several types of reaction in a conjugate system [33].

It is well known that the conjugated molecules are characterized by a small energy that separates the orbitals (HOMO-LUMO), which is the result of a significant degree of intramolecular charge transfer from the end-capping electron-donor groups to the acceptor groups by the conjugate route [34]. Therefore, the highest occupied molecular orbital (HOMO) and the lowest unoccupied molecular orbital (LUMO) are the main orbitals involved in chemical stability [35]. Thus, the energy gap gives an idea of the stability of the molecule. The HOMO represents the ability to donate an electron. However, the LUMO represents the ability to obtain an electron. The optimized structure of compound **1** and the HOMO and LUMO energies are shown in Figure 8.

The HOMO is located on the Cu, Cl and N atoms (Figure 8b and e), while the LUMO is located on the quinolone rings except nitrogen atoms (Figure 9c and f). The HOMO → LUMO transition involves an electron density transfer to the cyclic group from the CuN_4O_2 group.

$$E_{HOMO} = -4.95 eV$$

$$E_{LUMO} = -3.22 eV$$

$$\Delta E = E_{HOMO} - E_{LUMO} = -1.72 eV$$

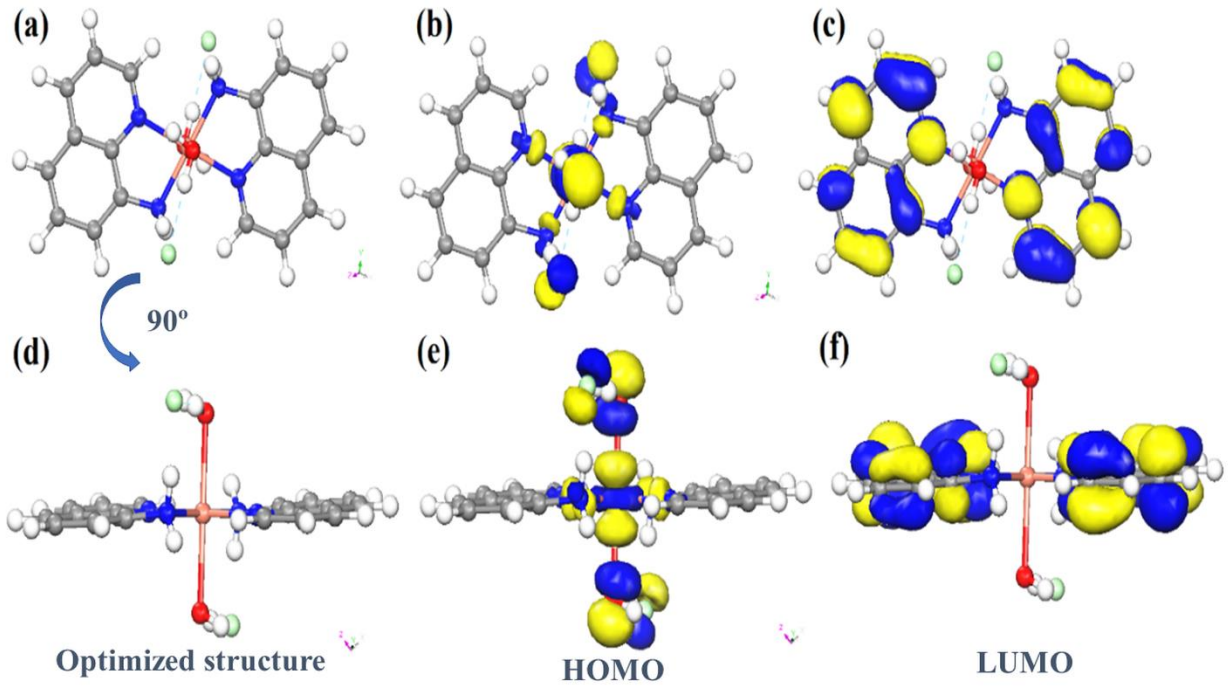

Figure 8. Optimized structure **(a)**, and Frontier molecular orbitals **[(b, e) HOMO and (c, f) (LUMO]** of **1**.

HOMO energy is directly related to ionization potential (IP), LUMO energy is directly related to electron affinity (EA) [36]:

$$IP = -E_{HOMO} = 4.95 \text{ eV}. \quad (1)$$

$$EA = -E_{LUMO} = 3.22 \text{ eV} \quad (2)$$

The Mulliken electronegativity (χ) and the Absolute hardness (η) can also deduced from the value of E_{HOMO} and E_{LUMO} as follow [37, 38]:

$$\chi = \frac{IP + EA}{2}, \quad \chi = -\frac{E_{LUMO} + E_{HOMO}}{2} = 4.09 \text{ eV} \quad (3)$$

$$\eta = \frac{IP - EA}{2}, \quad \eta = -\frac{E_{LUMO} - E_{HOMO}}{2} = 0.86 \text{ eV} \quad (4)$$

Fukui function

Fukui function is one of the most important factors for the determination of the chemical reactivity and the electrophilic and nucleophilic sites [39]. The Fukui indices as a function of the atomic charges are given by:

$$f_k^- = q_k(N) - (N-1) \text{ (for electrophilic attack)} \quad (5)$$

$$f_k^+ = q_k(N+1) - (N) \text{ (for nucleophilic attack)} \quad (6)$$

$$f_k^0 = [q_k(N+1) - q_k(N-1)]/2 \text{ (for radical attack)} \quad (7)$$

Where q_k is the electronic charge of atom k and N is the number of electrons. The values of the condensed Fukui function (f_k^-, f_k^+ , f_k^0), were calculated for electrophilic, nucleophilic, and radical attacks have been performed using Dmol[3] code. The results are summarized in Table 5.

Table 5 Fukui Indices for Radical Attack f_k^0, Nucleophilic Attack f_k^+ and for Electrophilic Attack f_k^-,

atom	f_k^0	f_k^+	f_k^-
Cu(1)	0.081	**0.117**	0.046
Cl(1)	0.042	0.030	0.054
Ow	0.003	0.003	0.004
Hw	0.006	0.006	0.006
Hw	0.014	0.016	0.013
N1	0.001	-0.006	0.008
N2	0.053	0.046	**0.059**
H	0.039	0.040	0.038
H	0.013	0.013	0.012
C1	0.026	0.028	0.024
H	0.027	0.028	0.026
C2	0.014	0.013	0.014
H	0.021	0.022	0.021
C3	0.026	0.027	0.025
H	0.019	0.020	0.019
C4	0.009	0.009	0.009
C5	0.020	0.020	0.021
H	0.019	0.018	0.019
C6	0.012	0.012	0.012
H	0.017	0.017	0.017
C7	0.022	0.022	0.023
H	0.021	0.021	0.021
C8	0.002	0.002	0.001
C9	0.032	0.034	0.030

The **Table 5** shows that the copper cation has highest value of f_k^+. Thus, this atom is the most favorite site for electrophilic attack. However, the nitrogen N2 presents the most favorite site for the nucleophile attack as it has the highest f_k^- value. Using the same reasoning, a radicular attack is very favored on copper. The results obtained from Fukui function and from the analysis of the LUMO and HOMO orbitals are in good agreement. The two methods lead to the same predictions of the sites which are most electron deficient.

Concluding Remarks

In summary, we have synthesized and structurally characterized a new copper (II) isomer $[Cu(H_2O)_2(C_9H_8N_2)_2]Cl_2$. The X-ray diffraction analysis shows that the coordination geometry around Cu atom has slightly distorted octahedral geometry. After formation of the coordination complex around the copper cation, the crystal packing is stabilized by two O-H···Cl^-, two N-H···Cl^- and five C-H···Cl^- (up to d_{HCl} = 3.36Å) hydrogen bonds as well as aromatic stacking interactions. The Hirshfeld surface analysis shows that the Cu(II)···N, Cu(II)···O, Ho/n···Cl^-, C···C, Hc···Cl^- and C···Hc are the most over-represented contacts, by decreasing order. The most important outcome of the theoretical calculations based on PBE functional method with DNP basis set, is the introduction of a new descriptor namely, Fukui indices. This descriptor is used to model chemical reactivity and site selectivity in **1**. The most important site for the nucleophilic attack of 1is the nitrogen atom of the quinolone rings,

whereas the preferred site for the electrophilic attack is the copper atom. The HOMO-LUMO energy gap and the different chemical reactivity descriptors show the intramolecular charge transfer taking place within the molecule and the significant antioxidant ability of **1**.

Availability of data and materials Experimental X-ray diffraction data are available from the Cambridge Crystallographic Data Centre on request quoting the deposition numbers CCDC 2054557.

Authors contributions

All authors, Z. Setifi, H. Ferjani, Y. Ben Smida, C. Jelsch, F. Setifi, C. Glidewell, made contributions to this study.

Funding The authors thank the Algerian Ministère de l'Enseignement Supérieur et de la Recherche Scientifique (MESRS), the Direction Générale de la Recherche Scientifique et du Développement Technologique (DGRSDT) as well as the Université Ferhat Abbas Sétif 1 for Financial support.

Data availability Data can be obtained from the corresponding authors through email.

Code availability Not applicable.

Declarations

Conflict of interest The authors declare no competing interests.

References

1. Setifi, Z., et al., 1,1'-Diethyl-4,4'-bipyridine-1,1'-diium bis(1,1,3,3-tetracyano-2-ethoxypropenide): multiple C-H...N hydrogen bonds form a complex sheet structure. Acta Crystallogr C Struct Chem, 2014. **70**(Pt 3): p. 338-41.
2. Benamara, N., et al., Coexistence of Spin Canting and Metamagnetism in a One-Dimensional Mn (II) Compound Bridged by Alternating Double End-to-End and Double End-On Azido Ligands and the Analog Co (II) Compound. Magnetochemistry, 2021. **7**(4): p. 50.
3. Dmitrienko, A.O., et al., Solid-state 1D→ 3D transformation of polynitrile-based coordination polymers by dehydration reaction. Dalton Transactions, 2020. **49**(21): p. 7084-7092.
4. Setifi, F., et al., Synthesis, structure, and magnetic properties of a dinuclear antiferromagnetically coupled iron (II) complex. Journal of Molecular Structure, 2017. **1149**: p. 149-154.
5. Setifi, Z., et al., Azide, water and adipate as bridging ligands for Cu(II) Synthesis, structure and magnetism of (μ4-adipato-κ-O)(μ-aqua)(μ-azido-κN1,N1)copper(II) monohydrate. Polyhedron, 2016. **117**: p. 244-248.
6. Benmansour, S., et al., Linkage isomerism in coordination polymers. Inorganic chemistry, 2012. **51**(4): p. 2359-2365.
7. Benmansour, S., et al., New coordination polymers based on a novel polynitrile ligand: Synthesis, structure and magnetic properties of the series [M (tcnoetOH) 2 (4, 4′-bpy)(H2O) 2](tcnoetOH−=[(NC) 2CC (OCH2CH2OH) C (CN) 2]−; M= Fe, Co and Ni). Inorganica Chimica Acta, 2008. **361**(14-15): p. 3856-3862.

8. Atmani, C., et al., New planar polynitrile dianion and its first coordination polymer with unexpected short M⋯ M contacts (tcno2−=[(NC) 2CC (O) C (CN) 2] 2−). Inorganic Chemistry Communications, 2008. **11**(8): p. 921-924.
9. Yan, L., et al., Cytotoxic palladium (II) complexes of 8-aminoquinoline derivatives and the interaction with human serum albumin. Journal of inorganic biochemistry, 2012. **106**(1): p. 46-51.
10. Zelenka, K., et al., Coordination chemistry and biological activity of 5′-OH modified quinoline–B12 derivatives. Dalton Transactions, 2011. **40**(38): p. 9665-9667.
11. Wang, K., M. Shen, and W.-H. Sun, Synthesis, characterization and ethylene oligomerization of nickel complexes bearing N-(2-(1 H-benzo [d] imidazol-2-yl) quinolin-8-yl) benzamide derivatives. Dalton Transactions, 2009(21): p. 4085-4095.
12. Setifi, F., et al., Spin Crossover Iron (II) Coordination Polymer Chains: Syntheses, Structures, and Magnetic Characterizations of [Fe (aqin) 2 (μ2-M (CN) 4)](M= Ni (II), Pt (II), aqin= Quinolin-8-amine). Inorganic chemistry, 2014. **53**(1): p. 97-104.
13. Genre, C., et al., First dicyanamide-bridged spin-crossover coordination polymer: synthesis, structural, magnetic, and spectroscopic studies. Chemistry–A European Journal, 2008. **14**(2): p. 697-705.
14. Genre, C., et al., A spin-crossover iron (ii) coordination polymer with the 8-aminoquinoline ligand: synthesis, crystal structure and magnetic properties of [Fe (aqin) 2 (4, 4′-bpy)](ClO 4) 2· 2EtOH (aqin= 8-aminoquinoline, 4, 4′-bpy= 4, 4′-bipyridyl). New Journal of Chemistry, 2006. **30**(11): p. 1669-1674.
15. Boonkitpatarakul, K., et al., An 8-aminoquinoline derivative as a molecular platform for fluorescent sensors for Zn (II) and Cd (II) ions. Journal of Luminescence, 2018. **198**: p. 59-67.
16. Morales, L., M.I. Toral, and M.J. Álvarez, A new Cu (II)-5-(4-sulphophenylazo)-8-aminoquinoline complex used for copper determination in presence of gold and silver in water and mineral samples. Talanta, 2007. **74**(1): p. 110-118.
17. Bortoluzzi, M., et al., Metal-assisted syntheses and NMR characterization of square-planar Pd (II) and Pt (II) complexes with tridentate nitrogen-donor chelate ligands. Inorganic Chemistry Communications, 2006. **9**(12): p. 1301-1303.
18. Rahmati, Z., et al., Accurate DFT studies on crystalline network formation of a new Co (II) complex bearing 8-aminoquinoline. Inorganica Chimica Acta, 2018. **473**: p. 152-159.
19. Paira, M., et al., Zn (II), Cd (II) and Hg (II) complexes of 8-aminoquinoline.: Structure, spectra and photoluminescence property. Polyhedron, 2007. **26**(15): p. 4131-4140.
20. CrysAlis, P., Agilent technologies. Yarnton, Oxfordshire, England, 2011.
21. Sheldrick, G.M., SHELXT–Integrated space-group and crystal-structure determination. Acta Crystallographica Section A: Foundations and Advances, 2015. **71**(1): p. 3-8.
22. Brandenburg, K. and H. Putz, Diamond. Crystal Impact GbR, Bonn, Germany, 2006.
23. Guillot, B., et al., MS19. O01. Acta Cryst, 2014. **70**: p. C279.
24. Delley, B., From molecules to solids with the DMol 3 approach. The Journal of chemical physics, 2000. **113**(18): p. 7756-7764.

25. Mulliken, R., Electronic population analysis on LCAO–MO molecular wave functions. II. Overlap populations, bond orders, and covalent bond energies. The Journal of Chemical Physics, 1955. **23**(10): p. 1841-1846.
26. Delley, B., Ground-state enthalpies: evaluation of electronic structure approaches with emphasis on the density functional method. The Journal of Physical Chemistry A, 2006. **110**(50): p. 13632-13639.
27. Xu, H. and C. Guo, catena-Poly [[(8-aminoquinoline-κ2N, N′) cadmium]-di-μ-thiocyanato-κ2N: S; κ2S: N-[(8-aminoquinoline-κ2N, N′) cadmium]-di-μ-chlorido]. Acta Crystallographica Section E: Structure Reports Online, 2012. **68**(1): p. m3-m3.
28. Kawamoto, K. and T. Shibahara, Trichlorido {2-dimethoxymethyl-4-methyl-6-[(quinolin-8-yl) iminomethyl] phenolato-κ3N, N′, O1} tin (IV). Acta Crystallographica Section E: Structure Reports Online, 2012. **68**(2): p. m208-m208.
29. Li, Z., et al., Bis [N-(8-quinolyl) pyridine-2-carboxamidato] iron (III) perchlorate monohydrate. Acta Crystallographica Section E: Structure Reports Online, 2007. **63**(11): p. m2781-m2781.
30. Kovbasyuk, L.A., O.A. Babich, and V.N. Kokozay, Direct synthesis and crystal structure of a mixed-valence copper complex. Polyhedron, 1997. **16**(1): p. 161-163.
31. Zhang, G., et al., Diverse copper (II) complexes with simple nitrogen ligands: Structural characterization and applications in aerobic alcohol oxidations in water. Polyhedron, 2016. **103**: p. 227-234.
32. Mao, R., et al., Decarboxylative C (sp 3)–N cross-coupling via synergetic photoredox and copper catalysis. Nature Catalysis, 2018. **1**(2): p. 120-126.
33. Fukui, K., T. Yonezawa, and H. Shingu, A molecular orbital theory of reactivity in aromatic hydrocarbons. The Journal of Chemical Physics, 1952. **20**(4): p. 722-725.
34. Choi, C.H. and M. Kertesz, Conformational information from vibrational spectra of styrene, trans-stilbene, and cis-stilbene. The Journal of Physical Chemistry A, 1997. **101**(20): p. 3823-3831.
35. Gunasekaran, S., et al., Experimental and theoretical investigations of spectroscopic properties of N-acetyl-5-methoxytryptamine. Can. J. Anal. Sci. Spectrosc, 2008. **53**(4): p. 149-162.
36. Gholami, M., et al., Correlated ab initio and electroanalytical study on inhibition behavior of 2-mercaptobenzothiazole and its thiole–thione tautomerism effect for the corrosion of steel (API 5L X52) in sulphuric acid solution. Industrial & Engineering Chemistry Research, 2013. **52**(42): p. 14875-14889.
37. Sastri, V. and J. Perumareddi, Molecular orbital theoretical studies of some organic corrosion inhibitors. Corrosion, 1997. **53**(08).
38. Pearson, R.G., Absolute electronegativity and hardness: application to inorganic chemistry. Inorganic chemistry, 1988. **27**(4): p. 734-740.
39. Lgaz, H., R. Salghi, and I.H. Ali, Corrosion inhibition behavior of 9-hydroxyrisperidone as a green corrosion inhibitor for mild steel in hydrochloric acid: electrochemical, DFT and MD simulations studies. Int. J. Electrochem. Sci, 2018. **13**: p. 250-264.

Supplementary Files

This is a list of supplementary files associated with this preprint. Click to download.

- SZ230.cif